RSC Advances

ROYAL SOCIETY OF CHEMISTRY

www.rsc.org/advances

Cite this: DOI: 10.1039/c0xx00000x

www.rsc.org/xxxxxx

ARTICLE

Cu(I) complex based on 6*H*-indolo[2,3-*b*]quinoxaline: structure and electrocatalytic property for hydrogen evolution reaction from water

Pan Zhang, [a] Xin Yang, [b] Penggang Jiang, [a] Junli Yin, [a] Yun Gong [*a] and Jianhua Lin [*a, c]

Received (in XXX, XXX) Xth XXXXXXXXX 20XX, Accepted Xth XXXXXXXXX 20XX
DOI: 10.1039/b000000x

Using a rigid ligand, 6*H*-indolo[2,3-*b*]quinoxaline (**HL**), a Cu(I) complex formulated as Cu_2L_2 (**1**) has been solvothermally synthesized and structurally characterized by single-crystal X-ray diffraction. The complex is a planar Cu_2 dimer, in which two Cu(I) ions are linked by two $\mathbf{L}^-$ with a Cu ··· Cu separation of 2.637 Å. And different Cu_2 units are connected by strong π-π stacking interactions into a three-dimensional (3D) supramolecular architecture. The **HL** ligand can't electrocatalyze the hydrogen evolution reaction (HER) from water, whereas the Cu(I) complex can act as an electrochemically stable electrocatalyst. In the presence of the Cu(I) complex, the exchanging current density i_0 for the HER is improved. And with the increase of the temperature, the HER current density is increased, and it is calculated the average activation energy E_a from 30 to 50 °C for the HER in the presence of the complex is ca. 40 kJ·mol^{-1}.

Introduction

In recent years, metal complexes attract people's great interest due to their intriguing variety of structures and interesting properties in catalysis, and porous materials, et al.[1] In particular, metal complexes have received more attention in electrochemical applications.[2] For example, Mao et al. used copper-based metal complexes as electrocatalysts in oxygen reduction reactions (ORR).[2a] Kumar et al. reported the electrocatalytic reduction of carbon dioxide at copper-based metal complex surface.[2b] In this regard, our research has been mainly focused on the synthesis and characterization of novel metal complexes to investigate their electrocatalytic activities for the H_2 evolution reaction (HER) from water.[3]

In our previous work, it is found that the species of metal(II) ions plays an important role in the electrocatalytic activity for the HER. [3] Usually the Co(II), Ni(II) or Cu(II) complex possesses the electrocatalytic activity for the HER, whereas the Zn(II) or Cd(II) complex doesn't have. And the sequence for the electrocatalytic activity is: Co(II) complex > Ni(II) complex > Cu(II) complex. [3] Metal complex is usually not electroconductive, which limits its uses in electrochemical field. To solve the problem, our strategy is to synthesize its graphene composite material to improve its electroconductivity. [3a] Lee et al. reported a composite material of graphene oxide and copper-centred metal complex, which shows good performances as a tri-functional electrocatalyst in the HER, oxygen evolution reaction (OER) and ORR.[2c]

However, the kinetic factor such as the activation energy E_a in the catalysis for the HER is still unexplored, herein, in order to investigate the relationship between the temperature and the electrocatalytic activity of metal complex for the HER, we synthesized a rigid ligand, 6*H*-indolo[2,3-*b*]quinoxaline (**HL**) (**Scheme 1**).[4] It is expected the ligand is stable under the electrochemical condition. Based on **HL**, we got a Cu(I) complex formulated as Cu_2L_2 (**1**). The cyclic voltammograms (CVs), Tafel plots, electrochemical impedance spectroscopies (EISs), controlled potential electrolysis (CPE) experiments under the temperature of 30, 50 and 80 °C as well as the UV-vis absorption spectra, electrochemical stability and thermal stability of the complex have been investigated.

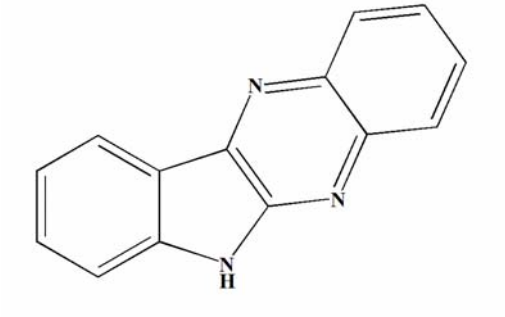

Scheme 1 Schematic representation of **HL**

Experimental Section

General Considerations All chemicals purchased were of reagent grade and used without further purification. The melting point was determined using an uncorrected X-4 melting point apparatus of Beijing Kaifu Company. C, H, N elemental analyses were performed on an Elementar Vario MICRO E III analyzer. IR spectra were recorded as KBr pellets on PerkinElmer spectrometer. The powder X-ray diffraction (PXRD) data were collected on a RIGAKU DMAX2500PC diffractometer using Cu Kα radiation. Thermogravimetric analysis (TGA) and simultaneous differential thermal analysis (DTA) were performed on a NETZSCH STA 449C thermogravimetric analyzer in flowing N_2 with a heating rate of 10°C·min^{-1}. The morphologies of the samples were characterized by SEM (Model JSM-7600F JEOL). UV-vis spectra were measured on a HITACHI U-4100 UV-vis spectro-photometer.

Electrochemical Measurements The electrochemical measurements were done in a three-electrode test cell using a Shiruisi RST5200 electrochemical workstation at 25 ℃.

saturated calomel electrode (SCE) and a platinum foil were used as the reference and counter electrode, respectively. The working electrode was prepared as follows: Firstly, a glassy carbon electrode (GCE) was polished by abrasive paper and aluminum oxide, then ultrasonically washed by ethanol, acetone and distilled water. Then an acetone dispersion of 4 mg **HL** or complex **1** and 0.05 mL of nafion were deposited on the GCE and the solvent is dried by an IR lamp. The electroactive geometric area of the GCE is 0.2 cm^2. The measurements were recorded in 50 mL of N_2 degassed 0.05 M phosphate buffer (pH = 6.8, 50 mL) aqueous solution. The amount of H_2 evolved was determined using gas chromatography (GC, 7890A, thermal conductivity detector (TCD), Ar carrier, Agilent). Electrochemical impedance spectroscopy (EIS) measurements were conducted on a CHI660E electrochemical workstation in the range of 0.01 Hz - 1 MHz, and the experimental conditions of EIS are as follows: The amplitude of the potential perturbation is 0.005V.

Synthesis of HL: HL was prepared according to the literature method.[4] Melting point: > 250℃.

Synthesis of Cu_2L_2 (1): A mixture of $Cu(NO_3)_2$ (0.09 mmol, 0.022 g), **HL** (0.06 mmol, 0.013 g) and DMF (8 mL) were placed in a Teflon-lined stainless steel vessel and heated at 150 °C for 3 days, followed by cooling to room temperature. The resulting brown block crystals were filtered off (yield: ca. 68 % based on **HL**). Elemental Anal. Found: C, 59.62; N, 14.90; H, 2.88 %. Calcd. for $C_{28}H_{16}Cu_2N_6$: C, 59.67; N, 14.91; H, 2.86 %. IR (cm^{-1}): 3444(s), 3062(m), 2365(m), 1625(m), 1605(s), 1558(s), 1511(m), 1485(s), 1468(m), 1450(s), 1428(s), 1380(m), 1339(m), 1295(m), 1248(m), 1210(s), 1137(m), 1037(m), 938(w), 850(w), 746(s), 575(w), 470(s).

X-ray crystallography Single-crystal X-ray data for **HL** and complex **1** were collected on an Oxford XCalibur Eos diffractometer using graphite monochromated Mo Ka (λ = 0.71073 Å) radiation at room temperature. Empirical absorption correction was applied. The structures were solved by direct methods and refined by the full-matrix least-squares methods on F^2 using the SHELXTL-97 software. [5] All non-hydrogen atoms were refined anisotropically. All of the hydrogen atoms were placed in the calculated positions. The crystal data and structure refinements for **HL** and complex **1** are summarized in **Table 1**. Selected bond lengths and angles for **HL** and complex **1** are listed in **Table S1** in the supporting information. The CCDC reference numbers are the following: 1046463 for **HL** and 800789 for complex **1**.

Table 1 Crystal data and structure refinements for **HL** and complex **1**

Complex	**HL**	**1**
Empirical formula	$C_{14}H_9N_3$	$Cu_2C_{28}H_{16}N_6$
M	219.24	563.55
Crystal system	monoclinic	monoclinic
Space group	$P2_1/n$	$P2_1/n$
a /Å	5.9177(5)	8.3236(3)
b /Å	9.092(8)	5.6787(2)
c /Å	18.7984(19)	22.6705(7)
α /º	90	90
β /º	91.9470(10)	90.581(3)
γ /º	90	90
V /Å^3	1010.9(9)	1071.52(6)
Z	4	2
D_{calcd}/g cm^{-3}	1.441	1.747
μ/mm^{-1}	0.089	2.018
No. of unique reflcns	1770	1887
reflcns used [$I > 2\acute{o}(I)$]	974	1238
F(0 0 0)	456	568
Goodness-of-fit on F^2	1.048	1.100
Final R indices [$I>2\sigma(I)$]	R_1= 0.0754, wR_2= 0.1659	R_1= 0.0472, wR_2= 0.1207

$R_1=\Sigma||F_0|-|F_c||/\Sigma|F_0|$; $wR_2=\Sigma[w(F_0^2-F_C^2)^2]/\Sigma[w(F_0^2)^2]^{1/2}$

Results and discussion

Crystal Structure of HL and Cu_2L_2 (1) Single-crystal X-ray diffraction analysis reveals that **HL** and complex **1** both crystallize in the *monoclinic* space group $P2_1/n$. In **HL**, there is one crystallographically independent **HL** molecule in the asymmetric unit. **HL** is a planar molecule with 1.346(5) and 1.392(5) Å of the two C-N distances in the pyrrole ring, and the two neighboring C-N bond lengths in the pyrazine ring are 1.314(5) and 1.376(5) Å, respectively (**Table S2**).

(a)

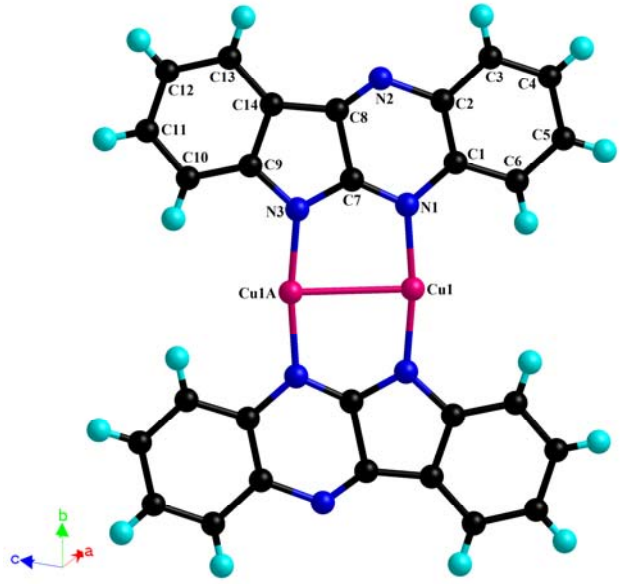

(b)

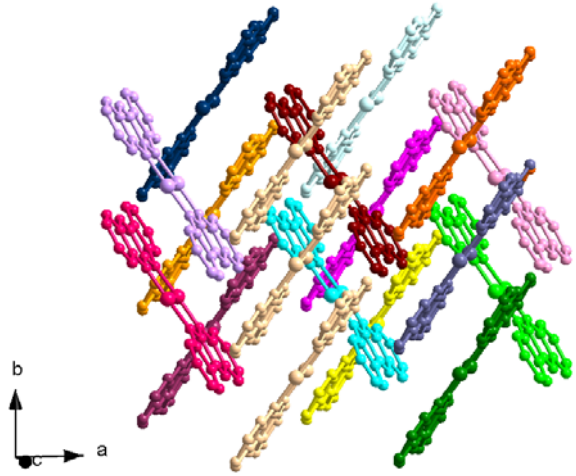

Fig. 1 Cu_2 unit constructed by Cu(I) and $\mathbf{L}^-$ in complex **1** (Atoms with additional label A refers to the symmetry operation: -*x*+2, -*y*-1, -*z*+2) (**a**); Cu_2 units are linked by strong π-π stacking interactions into 3D architecture (Different Cu_2 units denoted in different colors) (H atoms omitted for clarity) (**b**).

In complex **1**, the asymmetric unit contains one Cu (I) and one $\mathbf{L}^-$. As shown in **Fig. 1a**, in complex **1**, the crystallographically independent Cu(1) exhibits a linear geometry, defined by one pyrrole N atom and one pyrazine N atom from two $\mathbf{L}^-$ [Cu-N 1.863(4) - 1.889(4) Å] (**Fig. 1a**). Valences sum calculation shows that the Cu atom is in the +1 oxidation state [6] though the complex was synthesize based on Cu(II) salt. The work indicates that the Cu(II) ion in the starting material has been reduced to Cu(I) in the synthesis of the complex, which is because Cu(I) possesses more stable electron configuration ($3d^{10}$) than Cu(II).

In the complex, the $\mathbf{L}^-$ is planar with the H atom attached to the pyrrole N atom deprotonated. The C-N bond lengths in the pyrrole ring and pyrazine ring in $\mathbf{L}^-$ are 1.338(6), 1.405(6), 1.323(6) and 1.389(5) Å, respectively (**Table S2**), indicating the C-N distances in the $\mathbf{L}^-$ and **HL** ligands are a bit different, which is probably due to the difference of electron densities before and after the deprotonation. Two Cu(I) ions are linked by two $\mathbf{L}^-$ molecules via two pyrrole N atoms and two pyrazine N atoms into a Cu_2 unit with a Cu ⋯ Cu separation of 2.637(11) Å (**Fig. 1a**). And all the atoms in the Cu_2 unit are coplanar (**Fig. 1a**). Different units are connected by strong π-π stacking interactions (**Table S2**) into a three-dimensional (3D) supramolecular architecture (**Fig.1b**).

Thermal Stability of Complex 1 The powder X-ray diffraction (PXRD) of complex **1** is shown in **Fig. S1** in the supporting information. All the peaks of the compound can be indexed to the simulated XRD powder pattern, indicating the compound is pure phase. In order to examine the thermal stability of complex **1**, thermogravimetric analysis (TGA) and simultaneous differential thermal analysis (DTA) were carried out. The sample was heated up to 750 °C in N_2.

As shown in **Fig. 2**, no weight loss is observed from room temperature to 430 °C, which is in good agreement with the crystal structure of complex **1**, in which no solvent is included. The organic ligand began to be decomposed when the temperature is higher than 430 °C, and the calorimetric curve of complex **1** shows an obvious endotherm with a peak at 504 °C. The TGA curve of complex **1** shows that the compound possesses good thermal stability.

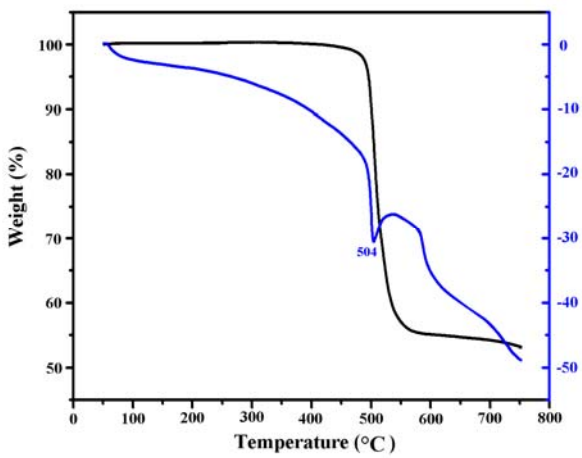

Fig. 2 TG and DTA curves for complex **1**.

The Electrochemical Property of HL and Complex 1 The electrochemical properties of **HL** and complex **1** were evaluated by cyclic voltammograms (CVs) in 0.05 M phosphate buffer aqueous solution (pH = 6.8, H_3PO_4/KOH, 50 mL) in a three-electrode cell with a SCE and a platinum foil were used as the reference and counter electrode, respectively. The CVs for the bare **GCE**, **HL**-modified glassy carbon electrode (**L-GCE**) and **1**-modified electrode (**1-GCE**) were measured. As shown in **Fig. 3** and **Fig. S2**, under the room temperature of 30 °C, the bare **GCE** exhibits the proton reduction at an onset potential of approximately -1.84 V vs SCE at a scan rate of 0.01 $V \cdot s^{-1}$. Since in a neutral aqueous solution (pH = 6.8), the theoretical potential for the H_2 evolution reaction (HER) on a clean Pt electrode is -0.64 V vs SCE,[7] the HER overpotential (η) at the bare **GCE** is 1.20 V vs SCE. The weak reduction peak at ca. -0.96 V vs SCE is probably associated with the impurity in the blank system. [3]

As shown in **Fig. 3** and **Fig. S3**, under the same temperature (30 °C) and at the same scan rate, the CVs reveal the proton reduction peak at **HL-GCE** was negatively shifted with respect to the bare **GCE**, indicating the free ligand **HL** can't catalyze the HER. And the irreversible reduction peak of the impurity in the blank system (-0.96 V vs SCE), is shifted to -0.86 V vs SCE in the presence of **HL** (**Fig. 3**).

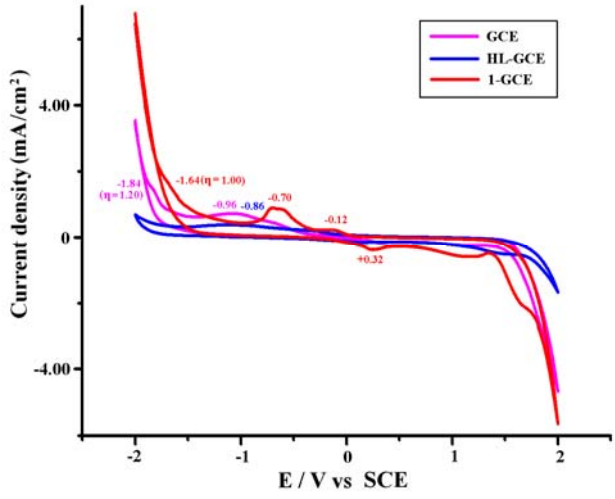

Fig. 3 CVs of the bare **GCE**, **HL-GCE** and **1-GCE** in 0.05M phospha

buffer aqueous solution (pH = 6.8, H_3PO_4/KOH, 50 mL) at a sweep rate of 0.01 V·s^{-1} at 30 ℃.

However, under the room temperature (30 °C), **1-GCE** shows the lower HER potential (-1.64 V vs SCE, η = 1.00 V) at 0.01 V·s^{-1} and the HER current density is enhanced with respect to the bare **GCE** (**Fig. 3** and **Fig. S4**), inferring that complex **1** can act as an electrocatalyst for the generation of H_2. [8] The quasi-reversible peaks at -0.12 and + 0.32 V vs SCE may be ascribed to the redox of Cu(I)/Cu(II) in complex **1** (**Fig. 3** and **Fig. S4**). [3c, 9] Similarly, the weak reduction peak at -0.70 V vs SCE is also probably associated with the redox of the impurity in the system.[3]

The electrocatalytic activity of complex **1** for the HER at 30 °C was also proved by the current intensity/overpotential diagram and the Tafel plot. As shown in **Fig. 4a** and **Fig. 4b**, when the scan rate is 0.01 V·s^{-1}, **1-GCE** shows lower overpotential and enhanced current density for the HER with respect to the bare **GCE**. According to $\eta = a + b\ log$ i, the intercept at the y axis $a = log\ i_0$ (i_0 is the exchanging current density), the slope b = 2.303RT/(αnF) (α is the charge-transfer efficiency).[10] As shown in **Fig. 4b**, in the presence of complex **1**, a = -4.4 and b = -0.66, it can be calculated α = 4.6 × 10^{-2} and i_0 = 4.0 × 10^{-5} A. Whereas without the electrocalalyst of complex **1**, a = -5.0 and b = -0.55, then α = 5.5 × 10^{-2} and i_0 = 1.0 × 10^{-5} A. The result indicates that the presence of complex **1** can improve the exchanging current density i_0 with respect to the bare **GCE**.

(**a**)

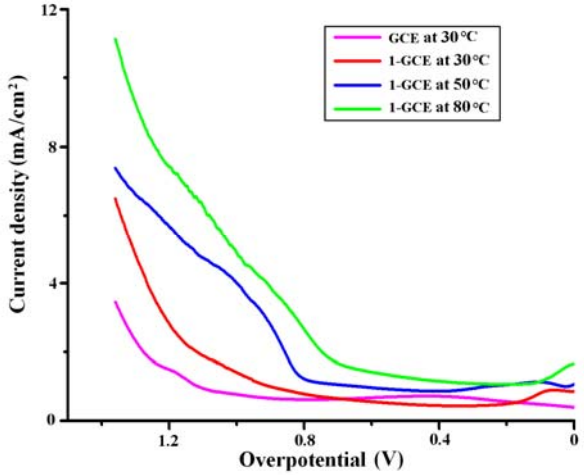

(**b**)

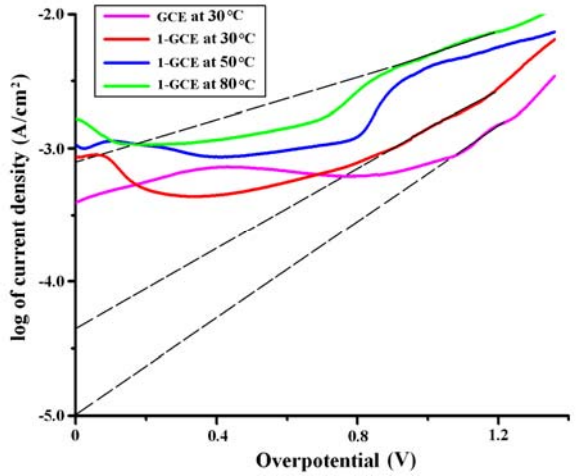

Fig. 4 Current intensity (i) / overpotential (η) diagrams (**a**) for the HER at the bare **GCE** and **1-GCE** in 0.05 M phosphate buffer aqueous solution (pH = 6.8, H_3PO_4/KOH, 50 mL) at sweep rates of 0.01 V·s^{-1} under different temperatures; Tafel plots of *logi* against overpotential η for the HER (The linear part of the Tafel curves denoted in black dotted lines with the intercept at the y axis) (**b**).

When the scan rate was changed to be 0.005 V·s^{-1}, similar phenomenon is also observed in the Tafel plot, as shown in **Fig. S5a**, in which the intercept $a = log\ i_0$ for **1-GCE** is also larger than the bare **GCE**, indicating the exchanging current density i_0 for the HER is improved at **1-GCE**.

At an electrolysis potential of -1.64 V vs SCE (η = 1.00 V), in the presence of complex **1**, with the increase of scan rate v, the ratio of the HER peak current i_p / square root of the scan rate $v^{1/2}$ is decreased (**Fig. S6**), indicating the rate determining step of the hydrogen evolution is electrochemical reaction.[10a]

The electrochemical impedance spectroscopy (EIS) of the complex was measured under the temperature of 30 °C. The Bode plots of **1-GCE** and the bare **GCE** at -1.5 V vs SCE are shown in **Fig. S7**. The R_s (electrolyte resistance) and the sum of R_s and R_{ct} (charge-transfer resistance) can be observed from the magnitude plot in the high and low frequency regions, respectively.[11] It is found that both the R_s and the sum of R_s and R_{ct} for the HER in the presence of complex **1** is lower than that in the blank system, indicating the resistance of the charge transfer is lowered in the presence of the complex.[11] It is probably associated with the Cu(I) ion in the complex, which function as the active center for the binding of intermediate species.[12]

Controlled potential electrolysis (CPE) experiment over 1 h at -1.5 V vs SCE (η = 0.86 V) under the temperature of 30 °C was performed to investigate the electrocatalytic property of the complex for the HER. As depicted in **Fig. S8a** and **Fig. S8b**, **1-GCE** shows more charge buildup versus time than the bare **GCE**, and larger HER current density is observed at **1-GCE** than the bare **GCE** under similar condition. And **CPE** experiment reveals the electrocatalyst of complex **1** operates at 98 % Faradaic efficiency for the HER (see ESI) with a turnover number (TON) of 1.2 mol of H_2 per mole of complex **1** at 30 °C.

(**a**)

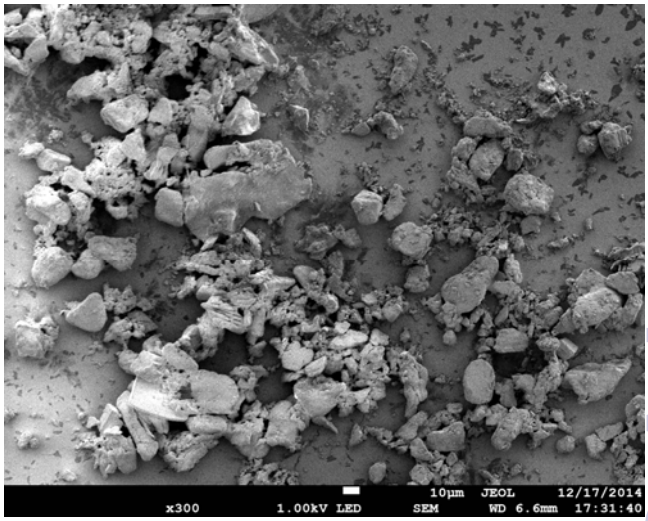

(**b**)

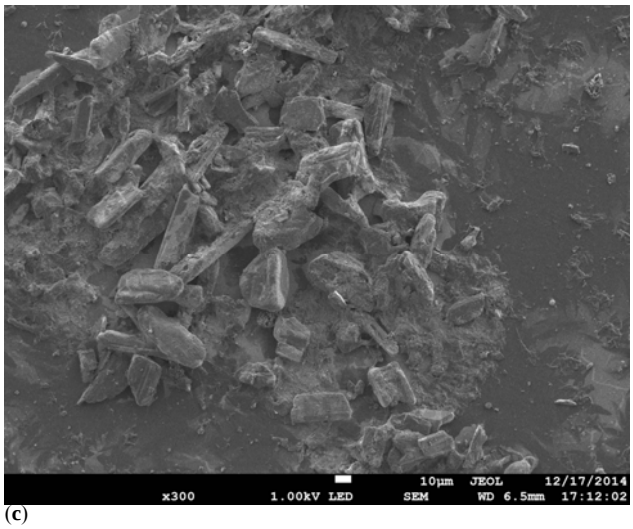

(**c**)

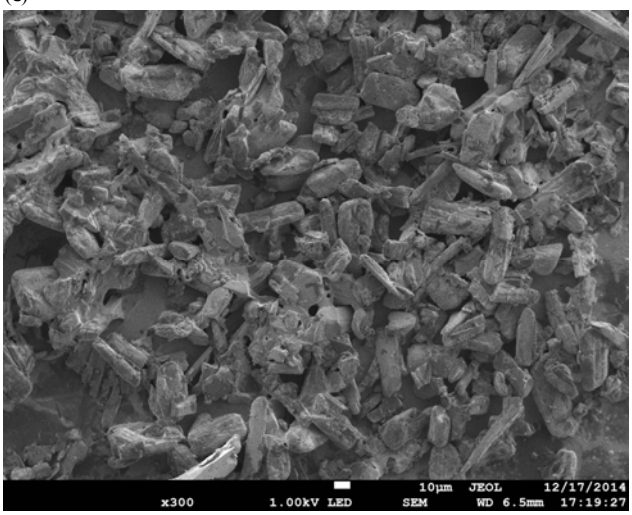

(**d**)

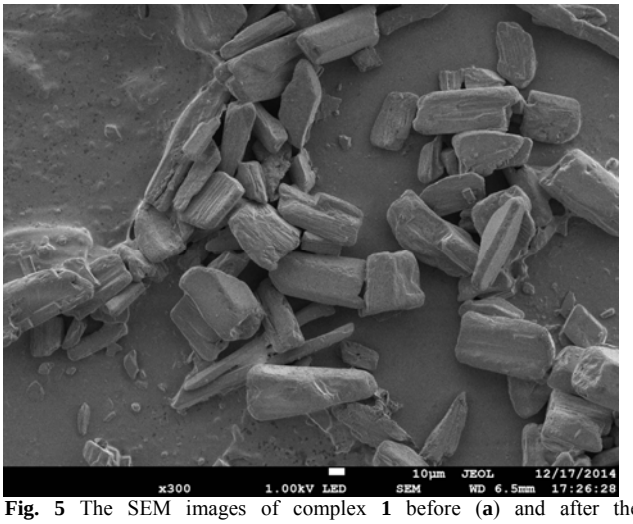

Fig. 5 The SEM images of complex **1** before (**a**) and after the electrochemical experiments at 30 °C (**b**), 50 °C (**c**) and 80 °C (**d**), respectively.

Moreover, **1-GCE** is stable. When the potential range is maintained at -2.0 to 2.0 V vs SCE, the peak current can be kept one hundred of cycles. After the CV cycles, the solid sample left on the **1-GCE** (**Fig. S9**) is characterized by the powder X-ray diffraction (PXRD) (**Fig. S1**), which displays a PXRD pattern similar to that of complex **1**, indicating the sample left on the electrode retain its structural integrity under the HER condition. The result is also proved by the SEM images of the sample before and after the electrochemical measurements. As shown in **Fig. 5** and **Fig. S10**, it is found that the morphologies of the sample are similar before and after the CV cycles.

The electrolyte solution before and after the CV cycles was characterized by UV-vis spectroscopy. As shown in **Fig. S11**, the solution exhibits similar absorption spectra before and after the electrochemical experiment, indicating complex **1** wasn't decomposed during the electrocatalytic process for the HER.

The Effect of Temperature on the Electrocatalytic Property of Complex 1 In order to investigate the effect of temperature on the electrocatalytic property of complex **1** for the HER, the CVs for **1-GCE** were also measured under similar condition at 50 and 80 °C, respectively.

As shown in **Fig. 6**, **Fig. S12** and **Fig. S13**, the quasi-reversible couple of -0.12/ + 0.32 V vs SCE at **1-GCE** under the temperature of 30 °C was shifted to -0.12/ + 0.17 and -0.07/ + 0.04 V vs SCE at 50 and 80 °C, respectively, which might be attributed to the redox of the Cu ion in complex **1**. [3c, 9] And the irreversible reduction peak was appeared at -0.70, -0.66 and -0.63 V vs SCE under the temperature of 30, 50 and 80 °C, respectively, which is probably ascribed to the redox of the impurity in the system.[3] As shown in **Fig. 6**, it is found that the HER current density is increased with the increase of the temperature. For example, when the scan rate is 0.01 $V \cdot s^{-1}$, at -1.64 V vs SCE (η = 1.00 V), as shown in **Fig. 4a**, the HER current density is 1.37 and 4.00 $mA \cdot cm^{-2}$ at 30 and 50 °C, respectively. According to Arhenius equation, $k = A\ exp\ (-E_a/RT)$, $ln\ (k_2/k_1) = E_a/R\ \{(T_2-T_1)/(T_1T_2)\}$, in which k_1 and k_2 are the rate constant at the temperature of T_1 and T_2, respectively. Herein, the rate constant is proportional to the HER current density. Then the average activation energy E_a in the temperature range from 30 to 50 °C is calculated to be 43.6 $kJ \cdot mol^{-1}$. Similarly, when the scan rate is 0.005 $V \cdot s^{-1}$, at the overpotential η of 1.00 V, as shown in **Fig. 5b**, the HER current density is 1.25 and 3.40 $mA \cdot cm^{-2}$ at 30 and 50 °C, respectively, and the E_a in the temperature range of 30-50 °C is calculated as 40.6 $kJ \cdot mol^{-1}$.

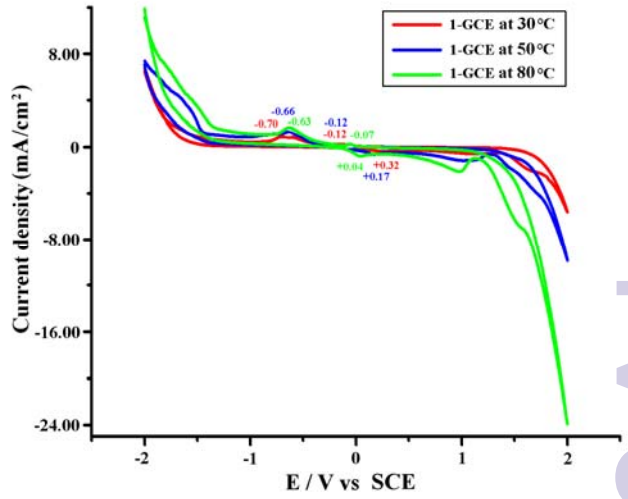

Fig. 6 CVs of **1-GCE** in 0.05 M phosphate buffer aqueous solution (pH = 6.8, H_3PO_4/KOH, 50 mL) at a sweep rate of 0.01 $V \cdot s^{-1}$ at 30 ℃ (red,

50 ℃ (blue) and 80 ℃ (green), respectively.

The Tafel plots at different temperatures are shown in **Fig. 4b**. It is found that at 80 °C, the incerpt a = -3.1 and the exchanging current density $i_0 = 7.9 \times 10^{-4}$ A, which is higher than the values at 30 °C (a = -5.0, $i_0 = 5.0 \times 10^{-5}$ A), indicating that with the increase of the temperature, the exchanging current density is increased.

The EISs of complex **1** at different temperatures are shown in **Fig. S7**. It is observed that both the R_s and the sum of R_s and R_{ct} for the HER at **1-GCE** are lowered with the increase of the temperature, indicating the increase of the temperature can prompt the diffusion of electrolyte and the transfer of charge.

The results of 1h-**CPE** at - 1.5 V vs SCE (η = 0.86 V) under different temperatures are in **Fig. S8**. **1-GCE** shows more charge buildup versus time and larger HER current density with the increase of the temperature. And complex **1** operates at 99 % Faradaic efficiencies for the HER (see ESI) with a TON of 2.7 and 4.6 mol of H_2 per mole of complex **1** at 50 and 80 °C, respectively.

As shown in **Fig. S1**, the solid sample left on the **1-GCE** after one hundred of CV cycles in the potential range of -2.0 ~ 2.0 V vs SCE at 50 and 80 °C also exhibits a PXRD pattern similar to that of complex **1**. And the sample can keep its morphology after the CV cycles at different temperatures, as shown in **Fig. 5** and **Fig. S10**, indicating the good electrochemical stability of complex **1** under different temperatures, which is probably associated with the quasi-reversible redox property of Cu(I)/Cu(II) in the complex (**Fig. 3** and **Fig. 6**).

UV-vis Absorption Spectra The UV-vis absorption spectra of the free organic ligand **HL** and complex **1** at room temperature are shown in **Fig. S14**. As shown in **Fig. S14**, the free ligand **HL** exhibits strong absorption peaks at ca. 250, 320 and 410 nm in the range of 230-500 nm, which may be ascribed to the n-π* or π-π* transition. [13] Complex **1** displays absorption peaks at ca. 280, 340 and 390 nm in the range of 230-500 nm. The absorption peaks for complex **1** is different from those of **HL**, indicating they may be ascribed to the intraligand transition (ILCT) or metal-to-ligand charge-transfer transition (MLCT). [13] In the range of 500-850 nm, **HL** and complex **1** show absorption peaks at ca. 535 and 550 nm, respectively, they may be ascribed to the visible *d* - *d* transition (**Fig. S14**).

Conclusion

Based on **HL**, a Cu(I) complex formulated as Cu_2L_2 (**1**) has been synthesized and structurally characterized by single-crystal X-ray diffraction. The complex is a planar Cu_2 dimer, in which two Cu(I) ions are linked by two $\mathbf{L}^-$ via two pyrrole N atoms and two pyrazine N atoms with a Cu ⋯ Cu separation of 2.637 Å. And different Cu_2 units are connected by strong π-π stacking interactions into a 3D supramolecular architecture.

The **HL** ligand can't electrocatalyze the HER from water, whereas the Cu(I) complex can act as the electrocatalyst, which is probably because the Cu(I) ion in the complex functions as the active center for the binding of intermediate species during the HER.[12] In the presence of the Cu(I) complex, both the R_s and the sum of R_s and R_{ct} for the HER are lowered, and the exchanging current density i_0 for the HER is improved. And with the increase of the temperature, the HER current density in the presence of the complex is increased, and it is calculated the average activation energy E_a in the temperature range from 30 to 50 °C for the HER is ca. 40 kJ· mol^{-1}. Before and after one hundred of CV cycles in the potential range of -2.0 ~ 2.0 V vs SCE, the sample on the electrode shows similar PXRD pattern and similar morphology, indicating the good electrochemical stability of the complex, which is probably associated with the quasi-reversible redox property of Cu(I)/Cu(II) in the complex.

Financial supports from the National Natural Science Foundation of China (No. 21371184), the Fundamental Research Funds for the Central Universities (no. CQDXWL-2012-024), the large-scale instrument and equipment open foundation in Chongqing University (No. 201406150041) and Chongqing Key Laboratory of Chemical Process for Clean Energy and Resource Utilization are gratefully acknowledged.

Notes and references

[a] *Department of Applied Chemistry, College of Chemistry and Chemical Engineering, Chongqing University, Chongqing 400030, P. R. China Tel: +86-023-65106150 E-mail: gongyun7211@cqu.edu.cn*
[b] *Chongqing Foreign Language School, Chongqing 400039, P. R. China*
[c] *State Key Laboratory of Rare Earth Materials Chemistry and Applications, College of Chemistry and Molecular Engineering, Peking University, Beijing 100871, P. R. China Tel: +86-010-62753541 E-mail: jhlin@pku.edu.cn; jhlin@cqu.edu.cn*

† Electronic Supplementary Information (ESI) available: [Crystallographic data; PXRD patterns; CVs; Tafel plots; Bode plots; CPE plots; SEM images; The images of electrode; UV-vis absorption spectra; The electrochemical property of nanosized Pt and other supplementary material]. See DOI: 10.1039/b000000x/

References

1 (a) M. W. Hosseini, *Acc. Chem. Res.*, 2005, **38**, 313; (b) P. J. Steel, *Acc. Chem. Res.*, 2005, **38**, 243; (c) C. Janiak, *Coord. Chem. Rev.,* 2006, **250**, 66; (d) F. Blank and C. Janiak, *Coord. Chem. Rev.,* 2009, **253**, 827; (e) X. C. Huang, Y. Y. Lin, J. P. Zhang and X. M. Chen, *Angew. Chem. Int. Ed.,* 2006, **45**, 1557; (f) Q. R. Fang, G. S. Zhu, Z. Jin, M. Xue, X. Wei, D. J. Wang and S. L. Qiu, *Angew. Chem. Int. Ed.,* 2006, **45**, 6126; (g) S. T. Zheng, J. Zhang, X. X. Li, W. H. Fang and G. Y. Yang, *J. Am. Chem. Soc.,* 2010, **132**, 15102.
2 (a) J. Mao, L. Yang, P. Yu, X. Wei and L. Mao, *Electrochem. Commun.*, 2012, **19**, 29; (b) R. Senthil Kumar, S. Senthil Kumar and M. Anbu Kulandainathan, *Electrochem. Commun*., 2012, **25**, 70; (c) M. Jahan, Z. Liu and K. P. Loh, *Adv. Funct. Mater*., 2013, **23**, 5363; (d) Y. F. Zhang, X. J. Bo, A. Nsabimana, C. Han, M. Li and L. P. Guo, *J. Mater. Chem. A*, 2015, **3**, 732; (e) M. Jahan, Q. L. Bao and K. P. Loh, *J. Am. Chem. Soc.*, 2012, **134**, 6707.
3 (a) X. L. Gao, Y. Gong, P. Zhang, Y. X. Yang, J. P. Meng, M. M. Zhang, J. L. Yin and J. H. Lin, *CrystEngComm*, 2014, **16**, 8492; (b) Y. Gong, M. M. Zhang, P. Zhang, H. F. Shi, P. G. Jiang and J. H. Lin, *CrystEngComm*, 2014, **16**, 9882; (c) Y. Gong, H. F. Shi, Z. Hao, W. Hua and J. H. Lin, *Cryst. Growth Des.,* 2014, **14**, 649.
4 (a) S. Takekuma, S. Katayama and H. Takekuma, *Chem. Lett.*, 2000, 614; (b) K. Niume, S. Kurosawa, F. Toda, M. Hasegawa and Y. Iwakura, *Bull. Chem. Soc. Jpn.*, 1982, **55**, 2293; (c) L. M. Wilhelmsson, N. Kingi and J. Bergman, *J. Med. Chem.,* 2008, **51**, 7744.
5 (a) G. M. Sheldrick, *SHELXS 97, Program for Crystal Structure Solution*, University of Göttingen, Göttingen, Germany, 1997. (b) G. M. Sheldrick, *SHELXL 97, Program for Crystal Structure Refinement*, University of Göttingen, Göttingen, Germany, 1997.
6 N. E. Brese and M. O'keeffe, *Acta Cryst.*, 1991, **B47**, 192.
7 B. Nohra, H. E. Moll, L. M. R. Albelo, P. Mialane, J. Marrot, C. M. Draznieks, M. O'Keeffe, R. N. Biboum, J. Lemaire, B. Keita, L. Nadjo and A. Dolbecq, *J. Am. Chem. Soc.*, 2011, **133**, 13363.
8 (a) L. Cheng, X. M. Zhang, X. D. Xi and S. J. Dong, *J. Electroanal.*

Chem. 1996, **407**, 97; (b) X. L. Wang, C. Qin, E. B. Wang, Z. M. Su, Y. G. Li and L. Xu, *Angew. Chem. Int. Ed.*, 2006, **45**, 7411; (c) P. P. Zhang, J. Peng, H. J. Pang, J. Q. Sha, M. Zhu, D. D. Wang and M. G. Liu, *CrystEngComm*, 2011, **13**, 3832; (d) L. F. Yang, S. Kinoshita, T. Yamada, S. Kanda, H. Kitagawa, M. Tokunaga, T. Ishimoto, T. Ogura, R. Nagumo, A. Miyamoto and M. Koyama, *Angew. Chem. Int. Ed*., 2010, **49**, 5348; (e) X. L. Wang, H. L. Hu, G. C. Liu, H. Y. Lin and A. X. Tian, *Chem. Commun*., 2010, **46**, 6485.

9 L. F. Yang, S. Kinoshita, T. Yamada, S. Kanda, H. Kitagawa, M. Tokunaga, T. Ishimoto, T. Ogura, R. Nagumo, A. Miyamoto and M. Koyama, *Angew. Chem. Int. Ed.,* 2010, **49**, 5348.

10 (a) H. Yang and W. Q. Lu, *Applied electrochemistry*, Science press, Beijing, 2001, 46; (b) Y. Gao and B. Wu, *Electrochemical Basis*, Chemical industry press, Beijing, 2003, 53.

11 (a) M. Hunsom, *Spectrosc. Prop. Inorg. Organomet. Compd.,* 2012, **42**, 196; (b) S. A. Mamuru, K. I. Ozoemena, T. Fukuda and N. Kobayashi, *J. Mater. Chem*., 2010, **20**, 10705; (c) S. Ghosh, R. K. Sahu and C. R. Raj, *J. Mater. Chem*., 2011, **21**, 11973; (d) M. K. Datta, K. Kadakia, O. I. Velikokhatnyi, P. H. Jampani, S. J. Chung, J. A. Poston, A. Manivannan and P. N. Kumta, *J. Mater. Chem. A,* 2013, **1**, 4026; (e) R. N. Reddy and R. G. Reddy, *J. Power Sources,* 2004, **132**, 315.

12 Koper, M. T. M.; Bouwman, E. *Angew. Chem. Int. Ed.,* 2010, **49**, 3723.

13 (a) S. Ohkoshi, H. Tokoro, T. Hozumi, Y. Zhang, K. Hashimoto, C. Mathonière, I. Bord, G. Rombaut, M. Verelst, C. C. Moulin and F. Villain, *J. Am. Chem. Soc.*, 2006, **128**, 270; (b) M. Stadler, F. Puntoriero, S. Campagna, N. Kyritsakas, R. Welter and J. M. Lehn, *Chem. Eur. J.*, 2005, **11**, 3997; (c) J. H. Wang, Y. Q. Fang, L. Bourget-Merle, M. I. J. Polson, G. S. Hanan, A. Juris, F. Loiseau and S. Campagna, *Chem. Eur. J.*, 2006, **12**, 8539.